Supporting Information: Topological Diagnosis of Polymer Composites via Inversion of Nonlinear Dielectric Mixing Rules

Proity Nayeeb Akbar

Department of Physics, Wesleyan University, 265 Church Street, Middletown, CT 06459-0155, USA

Email: pakbar@wesleyan.edu

Table of Contents:

Methods: Simulated Mixtures and Scattering Model

Starting with the experimental refractive index, $\tilde{n}(\tilde{\nu})$, of the individual polymers, the complex permittivity, $\tilde{\epsilon}_r(\tilde{\nu})$, of the materials is determined using:

$$\tilde{\epsilon}_r(\tilde{\nu}) = \tilde{\epsilon}_r^{'}(\tilde{\nu}) + i\tilde{\epsilon}_r^{''}(\tilde{\nu}) = \tilde{n}(\tilde{\nu})^2 = \{\tilde{n}^{'}(\tilde{\nu}) + i\tilde{n}^{''}(\tilde{\nu})\}^2, \quad (1)$$

$$\tilde{\epsilon}_r^{'}(\tilde{\nu}) = \tilde{n}^{'}(\tilde{\nu})^2 - \tilde{n}^{''}(\tilde{\nu})^2, \quad (2)$$

$$\tilde{\epsilon}_r^{''}(\tilde{\nu}) = 2\tilde{n}^{'}(\tilde{\nu})\tilde{n}^{''}(\tilde{\nu}), \quad (3)$$

where $\tilde{\epsilon}_r^{'}(\tilde{\nu})$, $\tilde{\epsilon}_r^{''}(\tilde{\nu})$, $\tilde{n}^{'}(\tilde{\nu})$, and $\tilde{n}^{''}(\tilde{\nu})$ represent the real and imaginary parts of $\tilde{\epsilon}_r(\tilde{\nu})$ and $\tilde{n}(\tilde{\nu})$, respectively, for a single polymer. The complex effective permittivity, $\tilde{\epsilon}_{eff}(\tilde{\nu})$, of a polymer mixture is described using inverted, logarithmic, and cubic mixing rules to account for nonlinear interactions within the components. These approximations model the complex multi-component spherical medium, where the properties of the composite system are governed by effective parameters.

As outlined below, equations (4) to (8) represent the complex effective permittivity, $\tilde{\epsilon}_{eff}^{(inverted)}(\tilde{\nu})$, obtained using the inverted mixing rule, equations (9) to (13) provides the complex effective

permittivity, $\tilde{\epsilon}_{eff}^{(log)}(\tilde{\nu})$, obtained using the logarithmic mixing rule, and equations (14) to (18) correspond to the complex permittivity, $\tilde{\epsilon}_{eff}^{(cubic)}(\tilde{\nu})$, given by the cubic mixing rule.

$$\frac{1}{\tilde{\epsilon}_{eff}^{(inverted)}(\tilde{\nu})} = \frac{1}{\tilde{\epsilon}_{eff}^{'(inverted)}(\tilde{\nu}) + i\tilde{\epsilon}_{eff}^{''(inverted)}(\tilde{\nu})} = \sum_{j=1}^{J} \frac{V_j}{\tilde{\epsilon}_{r_j}(\tilde{\nu})}, \tag{4}$$

$$\tilde{\epsilon}_{eff}^{'(inverted)}(\tilde{\nu}) = \frac{a_1}{a_1^2 + a_2^2}, \tag{5}$$

$$\tilde{\epsilon}_{eff}^{''(inverted)}(\tilde{\nu}) = \frac{a_2}{a_1^2 + a_2^2}, \tag{6}$$

$$a_1 = \sum_{j=1}^{J} \frac{V_j \tilde{\epsilon}_{r_j}^{'}(\tilde{\nu})}{\tilde{\epsilon}_{r_j}^{'}(\tilde{\nu})^2 + \tilde{\epsilon}_{r_j}^{''}(\tilde{\nu})^2}, \tag{7}$$

$$a_2 = \sum_{j=1}^{J} \frac{V_j \tilde{\epsilon}_{r_j}^{''}(\tilde{\nu})}{\tilde{\epsilon}_{r_j}^{'}(\tilde{\nu})^2 + \tilde{\epsilon}_{r_j}^{''}(\tilde{\nu})^2}. \tag{8}$$

$$\tilde{\epsilon}_{eff}^{(log)}(\tilde{\nu}) = \tilde{\epsilon}_{eff}^{'(log)}(\tilde{\nu}) + i\tilde{\epsilon}_{eff}^{''(log)}(\tilde{\nu}) = \prod_{j=1}^{J} \tilde{\epsilon}_{r_j}^{V_j}(\tilde{\nu}), \tag{9}$$

$$\tilde{\epsilon}_{eff}^{'(log)}(\tilde{\nu}) = \prod_{j=1}^{J} r_j^{V_j} \cos\left(\sum_{j=1}^{J} \theta_j V_j\right), \tag{10}$$

$$\tilde{\epsilon}_{eff}^{''(log)}(\tilde{\nu}) = \prod_{j=1}^{J} r_j^{V_j} \sin\left(\sum_{j=1}^{J} \theta_j V_j\right), \tag{11}$$

$$r_j(\tilde{\nu}) = \sqrt{\tilde{\epsilon}_{r_j}^{'}(\tilde{\nu})^2 + \tilde{\epsilon}_{r_j}^{''}(\tilde{\nu})^2}, \tag{12}$$

$$\theta_j(\tilde{\nu}) = \arctan\left(\frac{\tilde{\epsilon}_{r_j}^{''}(\tilde{\nu})}{\tilde{\epsilon}_{r_j}^{'}(\tilde{\nu})}\right), \tag{13}$$

$$\tilde{\epsilon}_{eff}^{(cubic)}(\tilde{\nu}) = \tilde{\epsilon}_{eff}^{'(cubic)}(\tilde{\nu}) + i\tilde{\epsilon}_{eff}^{''(cubic)}(\tilde{\nu}) = \left\{\sum_{j=1}^{J} V_j \tilde{\epsilon}_{r_j}^{\frac{1}{3}}(\tilde{\nu})\right\}^3, \tag{14}$$

$$\tilde{\epsilon}_{eff}^{'(cubic)}(\tilde{\nu}) = \sum_{j=1}^{J} \tilde{r}_j(\tilde{\nu}) cos\big(\tilde{\theta}_j(\tilde{\nu})\big), \tag{15}$$

$$\tilde{\epsilon}_{eff}^{''(cubic)}(\tilde{\nu}) = \sum_{j=1}^{J} \tilde{r}_j(\tilde{\nu}) sin\big(\tilde{\theta}_j(\tilde{\nu})\big), \tag{16}$$

$$\tilde{r}_j(\tilde{\nu}) = \left\{\sqrt{\left(\sum_{j=1}^{J} V_j r_j^{\frac{1}{3}} cos\left(\frac{\theta_j}{3}\right)\right)^2 + \left(\sum_{j=1}^{J} V_j r_j^{\frac{1}{3}} sin\left(\frac{\theta_j}{3}\right)\right)^2}\right\}^3, \tag{17}$$

$$\tilde{\theta}_j(\tilde{\nu}) = \arctan\left(\frac{\sum_{j=1}^{J} V_j r_j^{\frac{1}{3}} sin\left(\frac{\theta_j}{3}\right)}{\sum_{j=1}^{J} V_j r_j^{\frac{1}{3}} cos\left(\frac{\theta_j}{3}\right)}\right). \tag{18}$$

The quantities $\tilde{\epsilon}'^{(inverted)}_{eff}(\tilde{\nu})$, $\tilde{\epsilon}''^{(inverted)}_{eff}(\tilde{\nu})$, $\tilde{\epsilon}'^{(log)}_{eff}(\tilde{\nu})$, $\tilde{\epsilon}''^{(log)}_{eff}(\tilde{\nu})$, $\tilde{\epsilon}'^{(cubic)}_{eff}(\tilde{\nu})$, and $\tilde{\epsilon}''^{(cubic)}_{eff}(\tilde{\nu})$ express the real and imaginary components of $\tilde{\epsilon}^{(inverted)}_{eff}(\tilde{\nu})$, $\tilde{\epsilon}^{(log)}_{eff}(\tilde{\nu})$ and $\tilde{\epsilon}^{(cubic)}_{eff}(\tilde{\nu})$ for the inverted, logarithmic, and the cubic mixing rule, respectively. In this expression, $\tilde{\epsilon}_{r_j}(\tilde{\nu})$ and V_j denote the complex permittivity and volume fraction of the j-th polymer component in the composite system. The index j runs over the individual components of the mixture, with the total number of components given by J.

Methods: IR Measurements and Extinction Efficiency

The apparent IR absorbance, $A(\tilde{\nu})$, refers to the amount of infrared light transmitted by a material at specific wavenumbers, $\tilde{\nu}$, which provides information about its molecular structure and functional groups. Extinction efficiency, $Q_{ext}(\tilde{\nu})$, on the other hand, measures the effectiveness with which a material absorbs and scatters light. These two quantities are related by the following expression:

$$Q_{ext}(\tilde{\nu}) = \left(\frac{G}{g}\right)\left[1 - 10^{-A(\tilde{\nu})}\right], \tag{22}$$

$$A(\tilde{\nu}) = -\log_{10}\left[\frac{I(\tilde{\nu})}{I_0(\tilde{\nu})}\right], \tag{23}$$

where G is the reception area of the detector, and g is the geometric cross-section of the sample, with the condition that $G \gg g$. $I_0(\tilde{\nu})$ and $I(\tilde{\nu})$ are the intensities of the incident radiation and the transmitted radiation in the forward direction, respectively.

Methods: Inverse Reconstruction Pipeline

For a two-component mixture, the algorithm is initialized with a set of 30 dielectric functions, with initial conditions of $20\ cm^{-1}$ for all initial height $\tilde{\nu}_{p_{eff}}^{(n)}$ and width $\gamma_{eff}^{(n)}$. The position parameters $\tilde{\nu}_{0_{eff}}^{(n)}$ are initially distributed across the wavenumber interval $500\ cm^{-1} - 2200\ cm^{-1}$ ($20.0\ \mu m - 4.55\ \mu m$), with 25 dielectric functions allocated within this range, and the remaining 5 functions are placed in the range $2800\ cm^{-1} - 3500\ cm^{-1}$ ($3.57\ \mu m - 2.86\ \mu m$), where significant absorption is expected. The initial choice of ϵ_∞ is 2 and this is because most polymers typically have a DC-offset value that falls between 2 to 5.

For a multi-component mixture, while keeping everything else the same, the number of dielectric functions were increased to 34 with 30 dielectric functions distributed between $500\ cm^{-1}$ to $2200\ cm^{-1}$ ($20.0\ \mu m$ to $4.55\ \mu m$) and the remaining 4 functions positioned in the range $2800\ cm^{-1} - 3500\ cm^{-1}$ ($3.57\ \mu m - 2.86\ \mu m$).

Methods: Accuracy and Sensitivity Testing

Due to its nonlinear iterative nature, the reconstruction algorithm exhibits a high sensitivity to the initial conditions. Consequently, the reconstructed effective permittivity, $\tilde{\epsilon}_{eff}^{(model)}(\tilde{\nu})$, is influenced by the initial values chosen for the unknown parameters, $\left\{\epsilon_{\infty}, \tilde{\nu}_{0_{eff}}^{(n)}, \tilde{\nu}_{p_{eff}}^{(n)}, \gamma_{eff}^{(n)}\right\}$, within the nonlinear reconstruction framework. To evaluate the robustness, accuracy, and precision of our reconstruction method, we performed numerous reconstructions of the volume fractions, V_j, for multi-component dielectric materials. This process involved spectral inversion followed by mixture deconvolution using both grid search and gradient descent techniques. During these reconstructions, we varied the initial conditions for the parameters, $\tilde{\nu}_{p_{eff}}^{(n)}$, which were randomly sampled from an exponential distribution over the interval $[0, \infty)$, with a rate parameter of $\lambda = 10$, resulting in a mean value of 0.1. This choice of rate parameter ensures that the generated $\tilde{\nu}_{p_{eff}}^{(n)}$ values are uncorrelated and tend to be smaller, which aligns with the expected absorption characteristics of the materials being studied, especially their typical IR spectral features. Since the height of a dielectric function is related to its width through the full width at half maximum (FWHM) definition, where the width is taken at the half-height point of the peak, we believe it is sufficient to adjust either parameter, $\tilde{\nu}_{p_{eff}}^{(n)}$ or $\gamma_{eff}^{(n)}$, to observe their effect on the reconstruction.

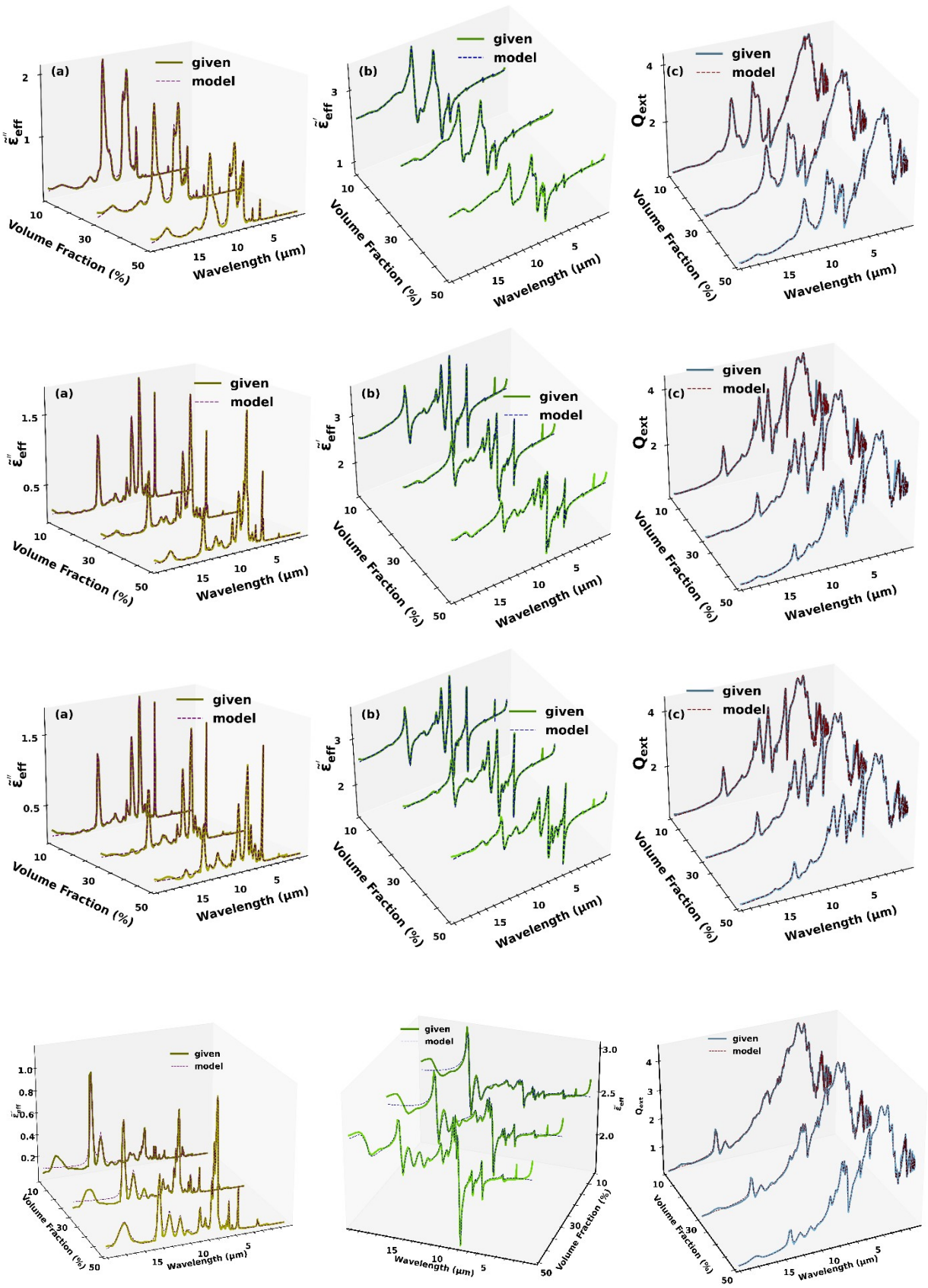
(a)
given
model
Volume Fraction (%)
Wavelength (μm)
(b)
given
model
Volume Fraction (%)
Wavelength (μm)
(c)
given
model
Volume Fraction (%)
Wavelength (μm)
(a)
given
model
Volume Fraction (%)
Wavelength (μm)
(b)
given
model
Volume Fraction (%)
Wavelength (μm)
(c)
given
model
Volume Fraction (%)
Wavelength (μm)
(a)
given
model
Volume Fraction (%)
Wavelength (μm)
(b)
given
model
Volume Fraction (%)
Wavelength (μm)
(c)
given
model
Volume Fraction (%)
Wavelength (μm)
given
model
Volume Fraction (%)
Wavelength (μm)
given
model
Wavelength (μm)
Volume Fraction (%)
given
model
Volume Fraction (%)
Wavelength (μm)

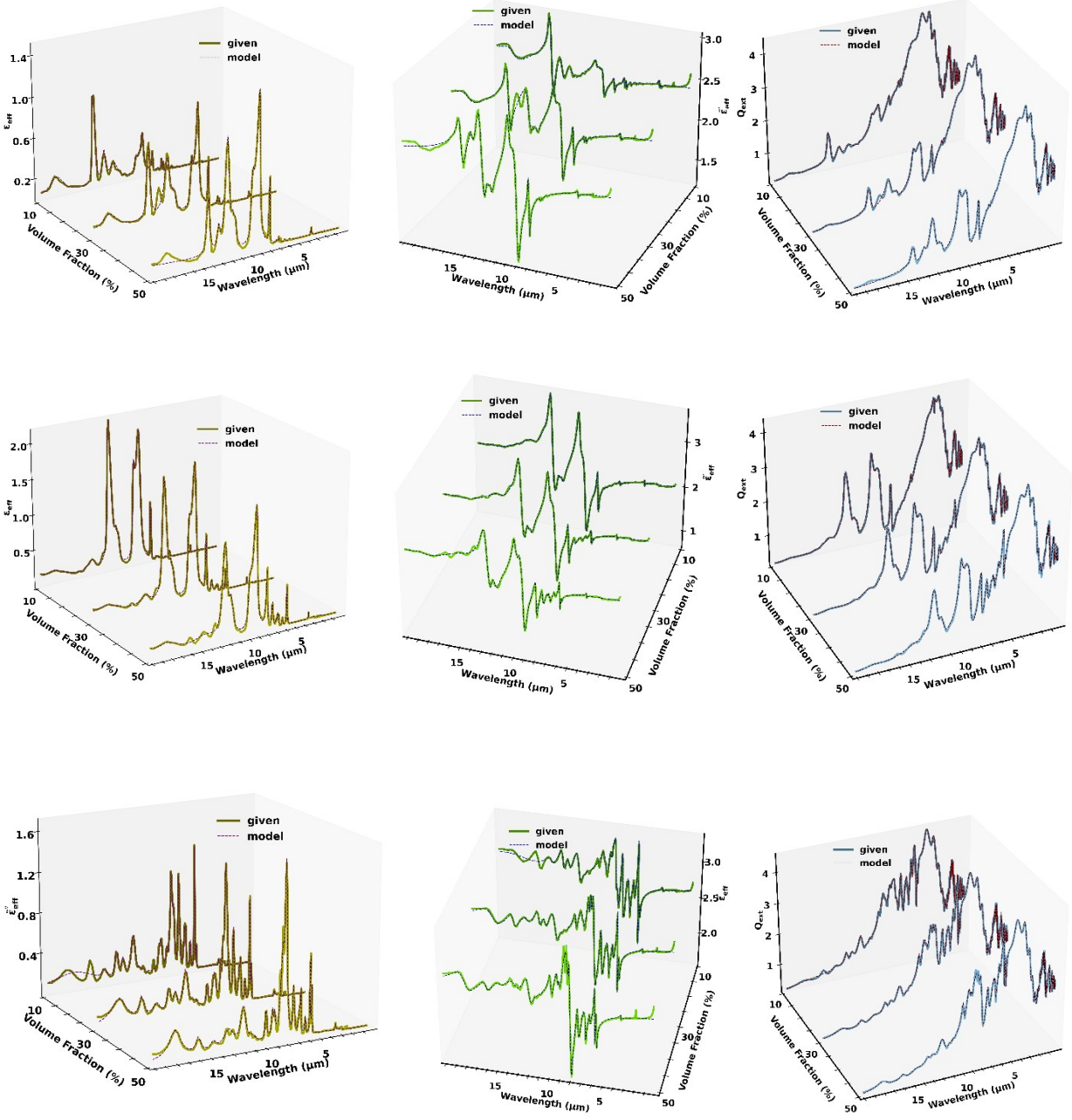
given
model
Volume Fraction (%)
Wavelength (μm)

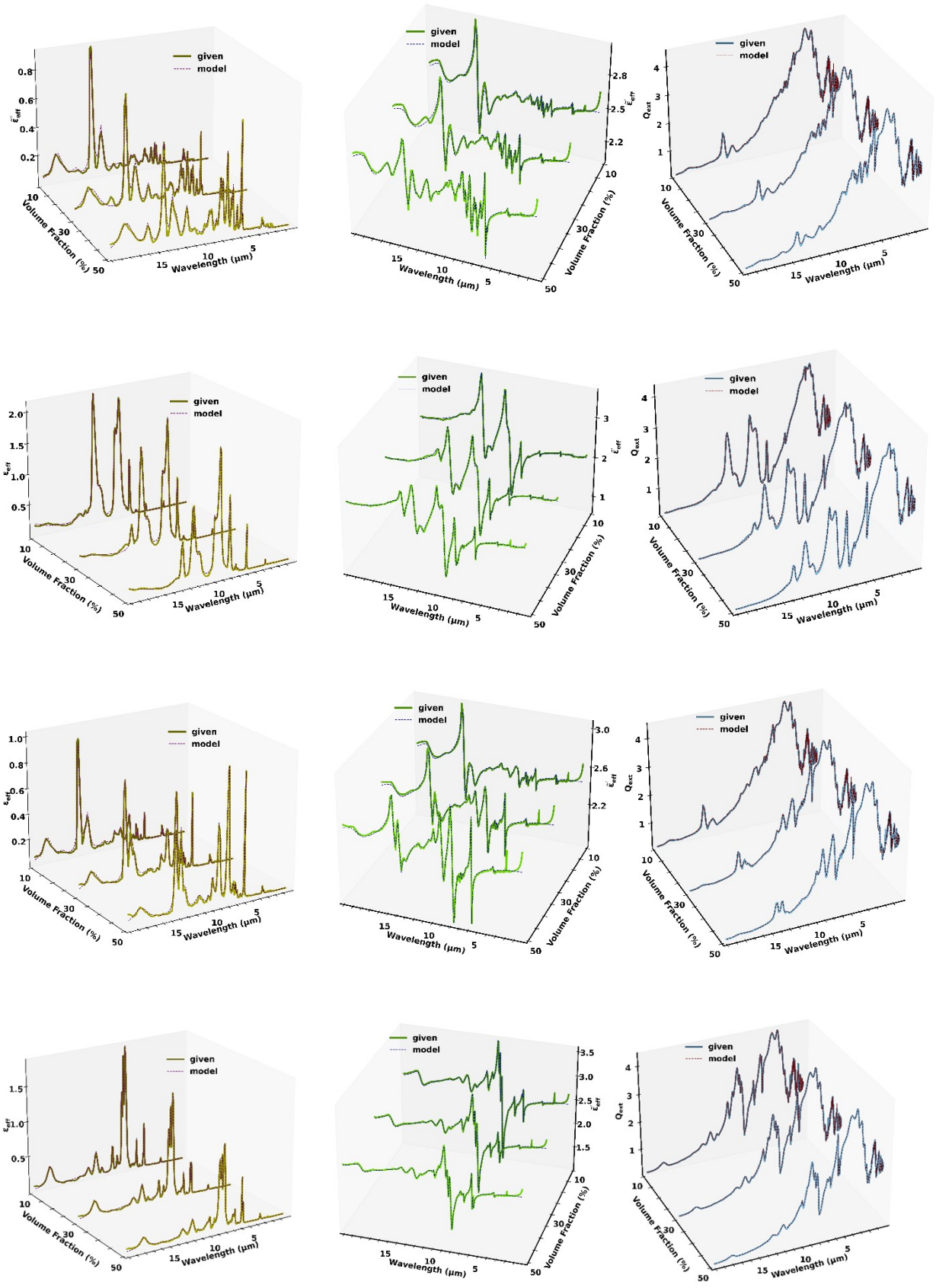
given
model
Volume Fraction (%)
Wavelength (μm)
$\tilde{\varepsilon}_{eff}$
Q_{ext}

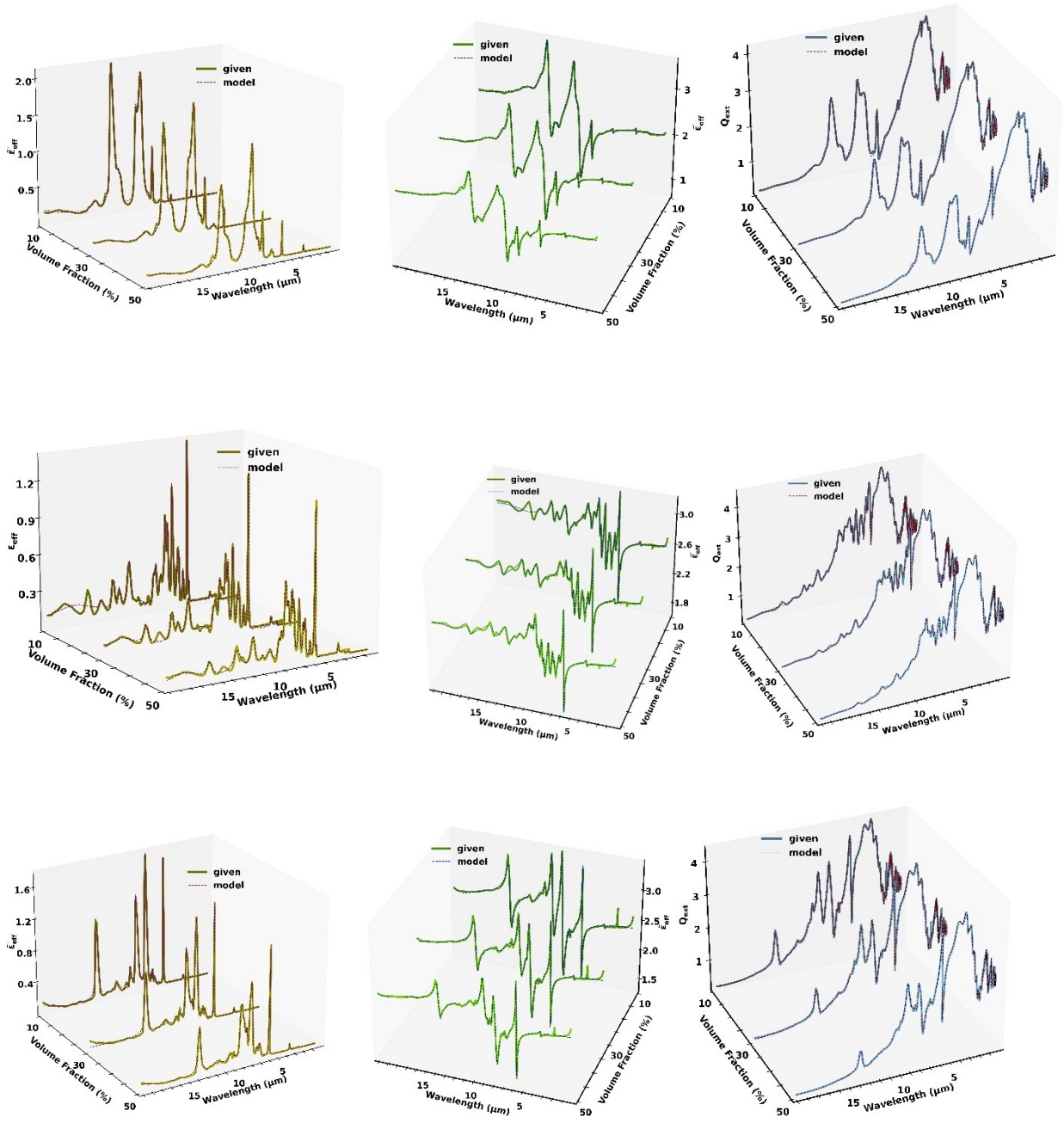
given
model
Volume Fraction (%)
Wavelength (μm)
$\bar{\varepsilon}_{eff}$
Q_{ext}

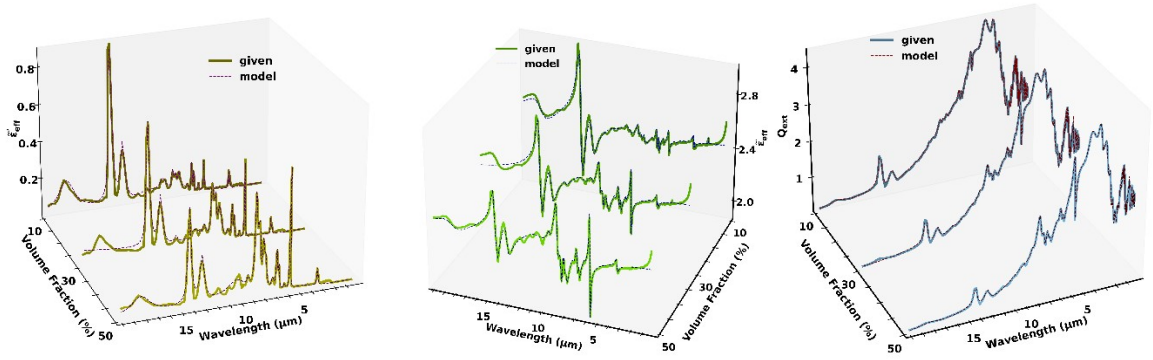

Figure S1 Compares the **(a)** imaginary (solid pale yellow) part of the experimental complex effective permittivity, $\tilde{\epsilon}_{eff}^{''}$, to the imaginary (dashed yellow) part of the fit of the complex effective permittivity, $\tilde{\epsilon}_{eff}^{''(model)}$, **(b)** real (solid pale green) part of the experimental complex effective permittivity, $\tilde{\epsilon}_{eff}^{'}$, to the real (dashed dark blue) part of the fit of the complex effective permittivity, $\tilde{\epsilon}_{eff}^{'(model)}$, and **(c)** experimental effective extinction efficiency (solid light blue), $Q_{ext}^{(given)}$, to the numerical fit of the effective extinction efficiency (dashed dark red), $Q_{ext}^{(model)}$, respectively, for three two-component inverted mixtures, each composed of 10% − 90%, 30% − 70%, and 50% − 50% of **A)** PC-PDMS, **B)** PC-PET, **C)** PEI-PET, **D)** PC-PS, **E)** PDMS-PS, **F)** PEI-PDMS, **G)** PC-PEI, **H)** PEI-PS, **I)** PET-PDMS, **J)** PET-PS, **K)** PMMA-PC, **L)** PMMA-PDMS, **M)** PMMA-PEI, **N)** PMMA-PET, and **O)** PMMA-PS, respectively.

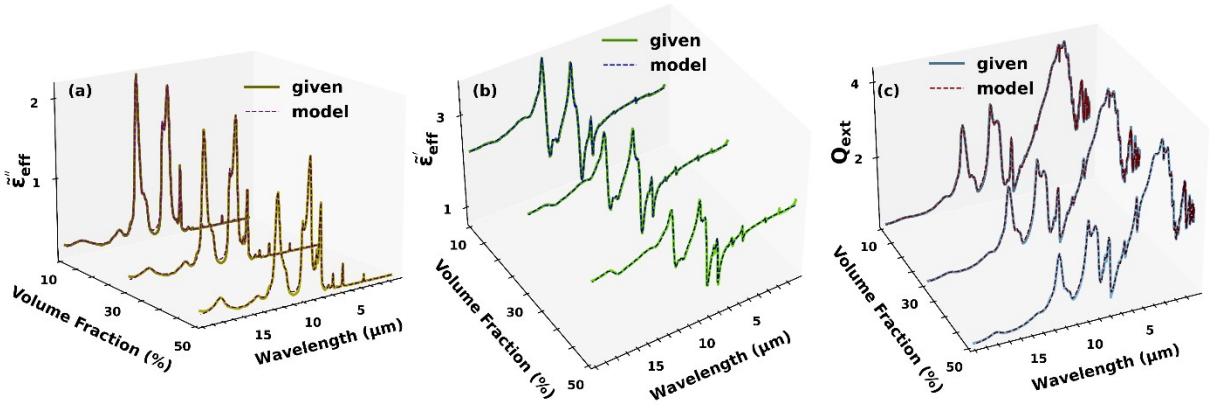
(a)
given
model
$\tilde{\varepsilon}''_{eff}$
Volume Fraction (%)
Wavelength (μm)
(b)
given
model
$\tilde{\varepsilon}'_{eff}$
Volume Fraction (%)
Wavelength (μm)
(c)
given
model
Q_{ext}
Volume Fraction (%)
Wavelength (μm)

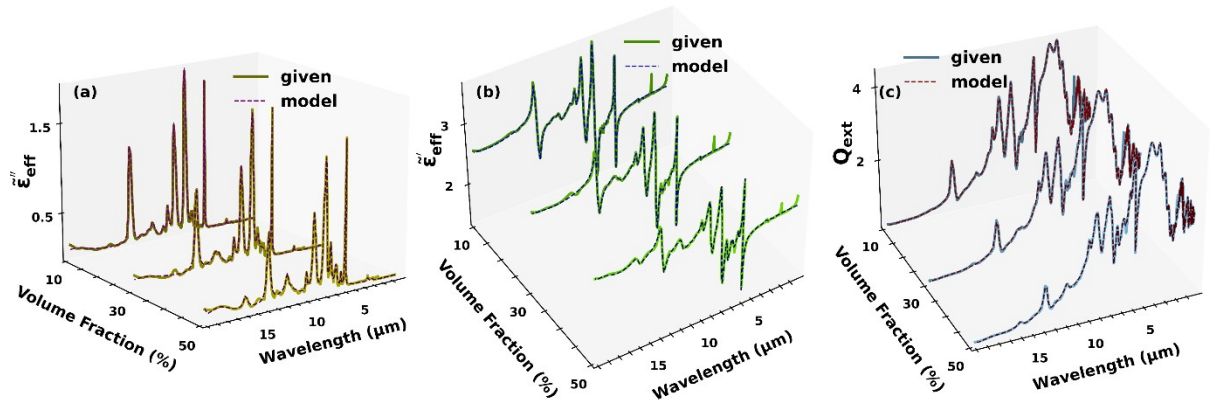
(a)
given
model
$\tilde{\varepsilon}''_{eff}$
Volume Fraction (%)
Wavelength (μm)
(b)
given
model
$\tilde{\varepsilon}'_{eff}$
Volume Fraction (%)
Wavelength (μm)
(c)
given
model
Q_{ext}
Volume Fraction (%)
Wavelength (μm)

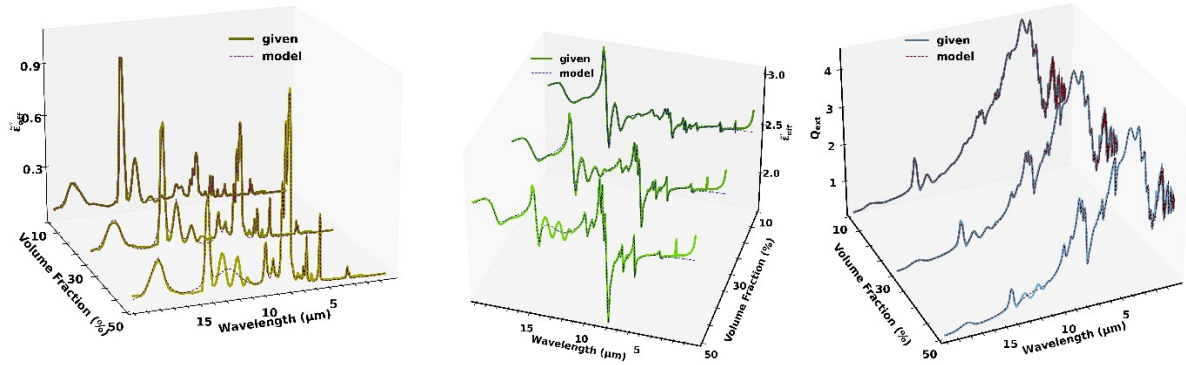
given
model
Volume Fraction (%)
Wavelength (μm)
given
model
Wavelength (μm)
Volume Fraction (%)
given
model
Q_{ext}
Volume Fraction (%)
Wavelength (μm)

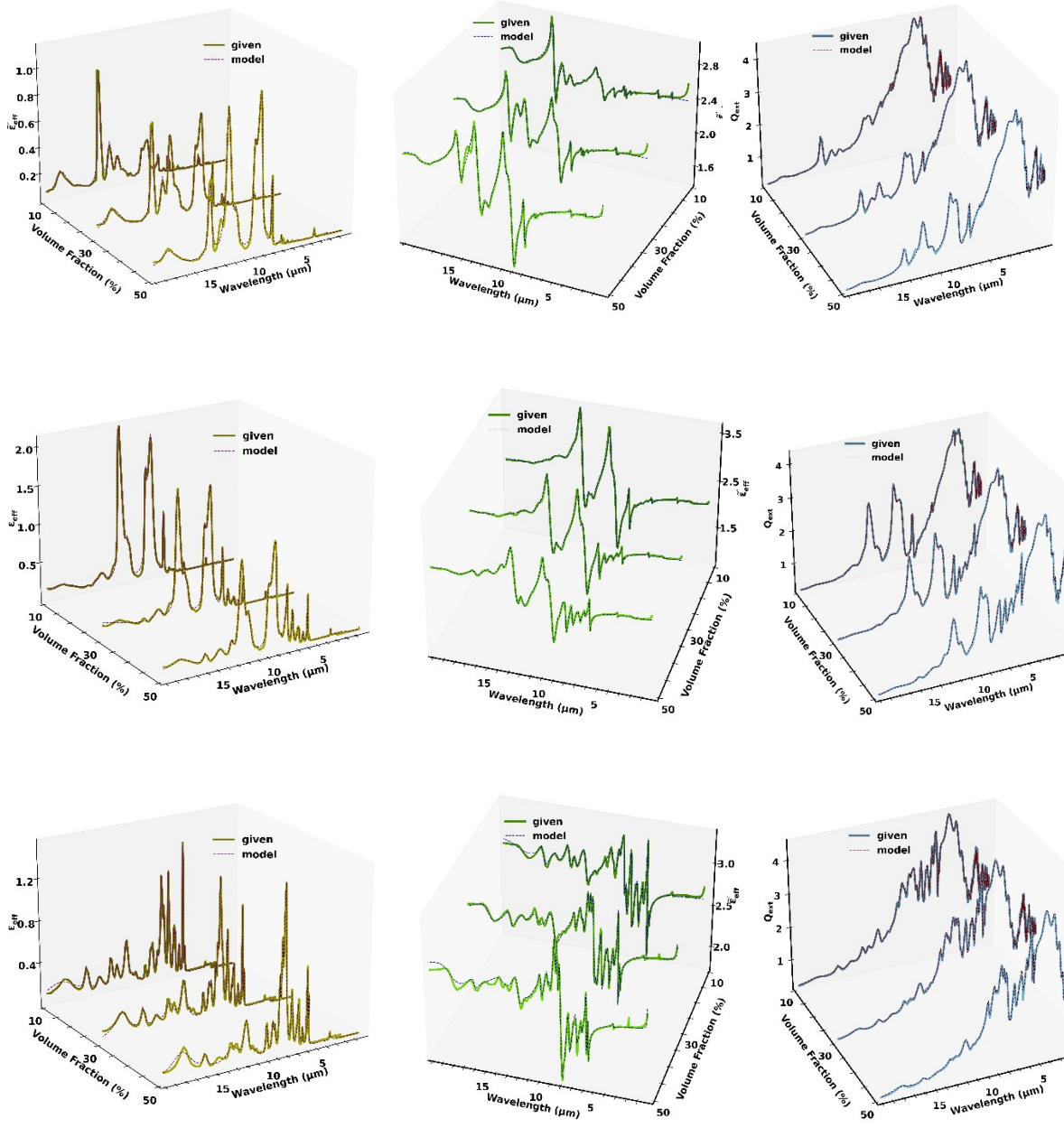
given
model
Volume Fraction (%)
Wavelength (μm)
Q_{ext}
$\tilde{\varepsilon}_{eff}$

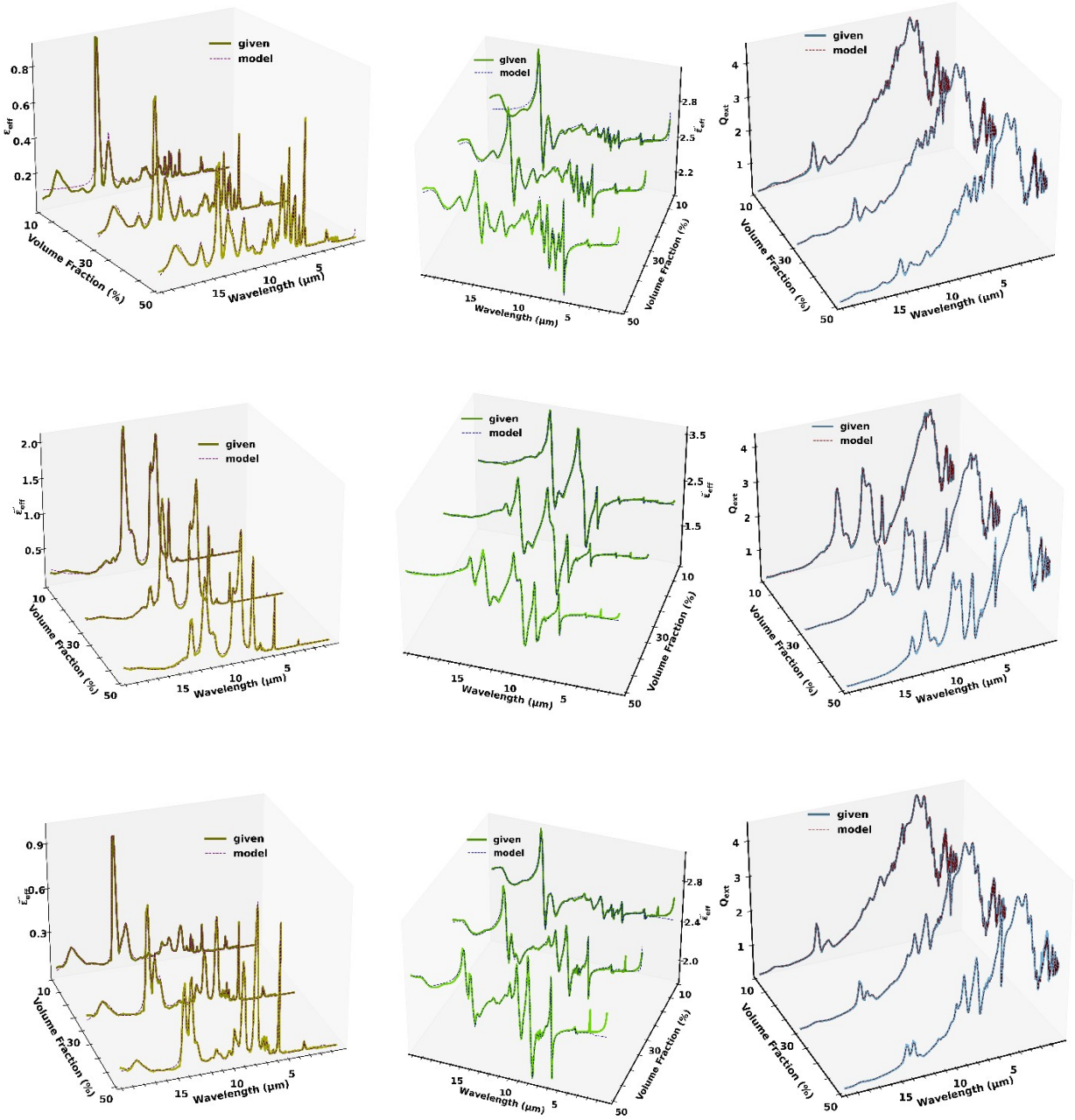
given
model
Volume Fraction (%)
Wavelength (μm)
$\tilde{\varepsilon}_{eff}$
Q_{ext}

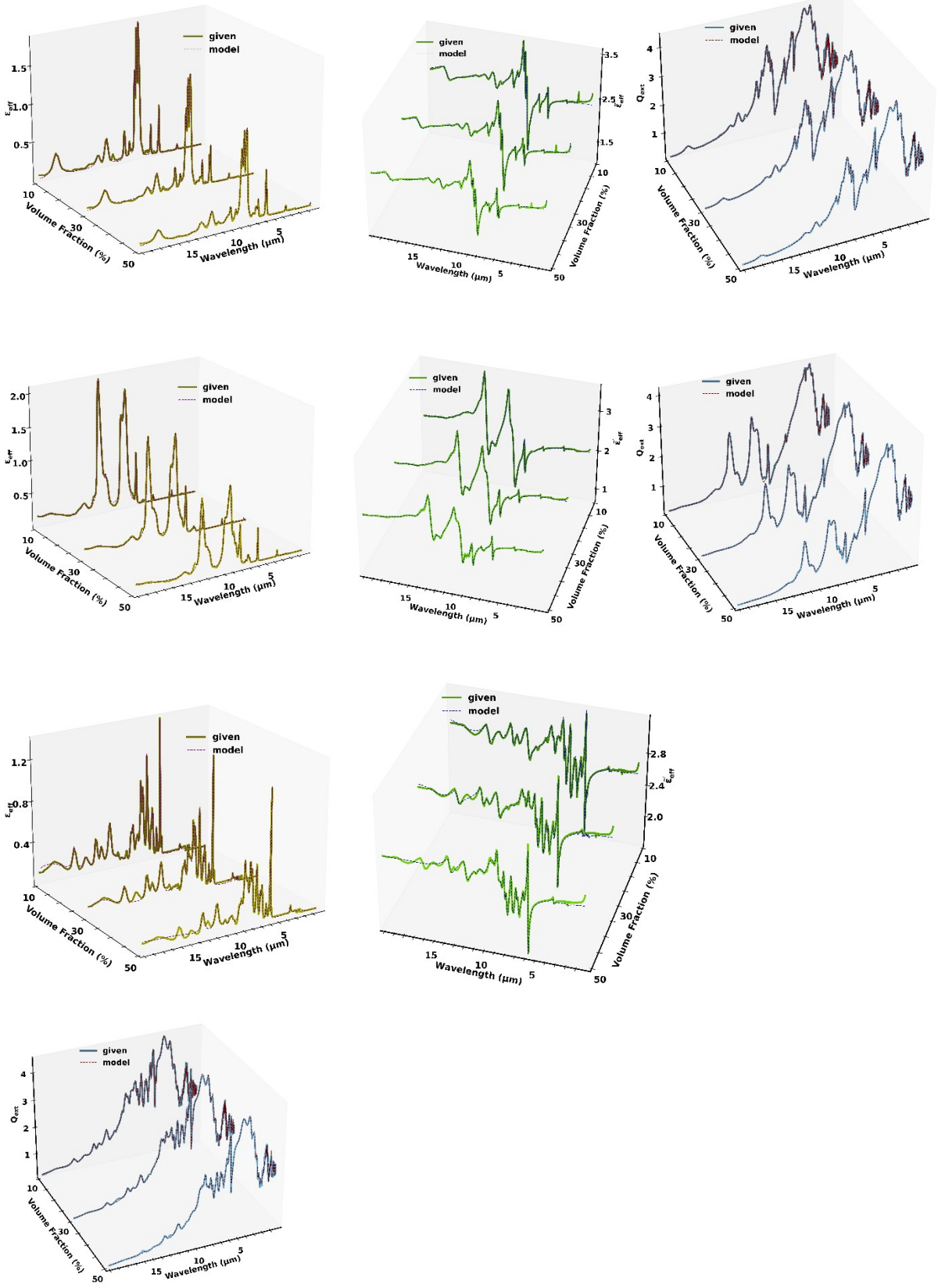
given
model
Volume Fraction (%)
Wavelength (μm)
Qext
εeff

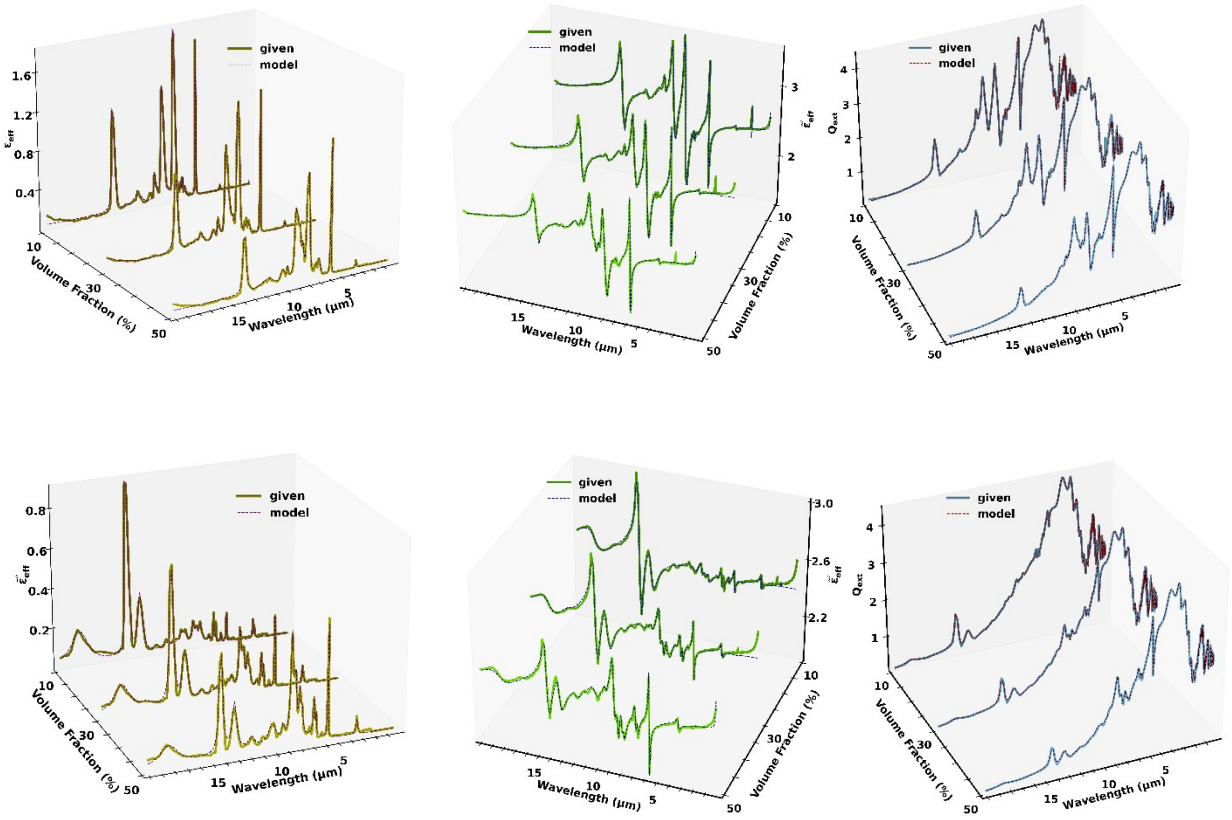

Figure S2 Compares the **(a)** imaginary (solid pale yellow) part of the experimental complex effective permittivity, $\tilde{\epsilon}_{eff}^{''}$, to the imaginary (dashed yellow) part of the fit of the complex effective permittivity, $\tilde{\epsilon}_{eff}^{''(model)}$, **(b)** real (solid pale green) part of the experimental complex effective permittivity, $\tilde{\epsilon}_{eff}^{'}$, to the real (dashed dark blue) part of the fit of the complex effective permittivity, $\tilde{\epsilon}_{eff}^{'(model)}$, and **(c)** experimental effective extinction efficiency (solid light blue), $Q_{ext}^{(given)}$, to the numerical fit of the effective extinction efficiency (dashed dark red), $Q_{ext}^{(model)}$, respectively, for three two-component logarithmic mixtures, each composed of $10\% - 90\%$, $30\% - 70\%$, and $50\% - 50\%$ of **A)** PC-PDMS, **B)** PC-PET, **C)** PEI-PET, **D)** PC-PS, **E)** PDMS-PS, **F)** PEI-PDMS, **G)** PC-PEI, **H)** PEI-PS, **I)** PET-PDMS, **J)** PET-PS, **K)** PMMA-PC, **L)** PMMA-PDMS, **M)** PMMA-PEI, **N)** PMMA-PET, and **O)** PMMA-PS, respectively.

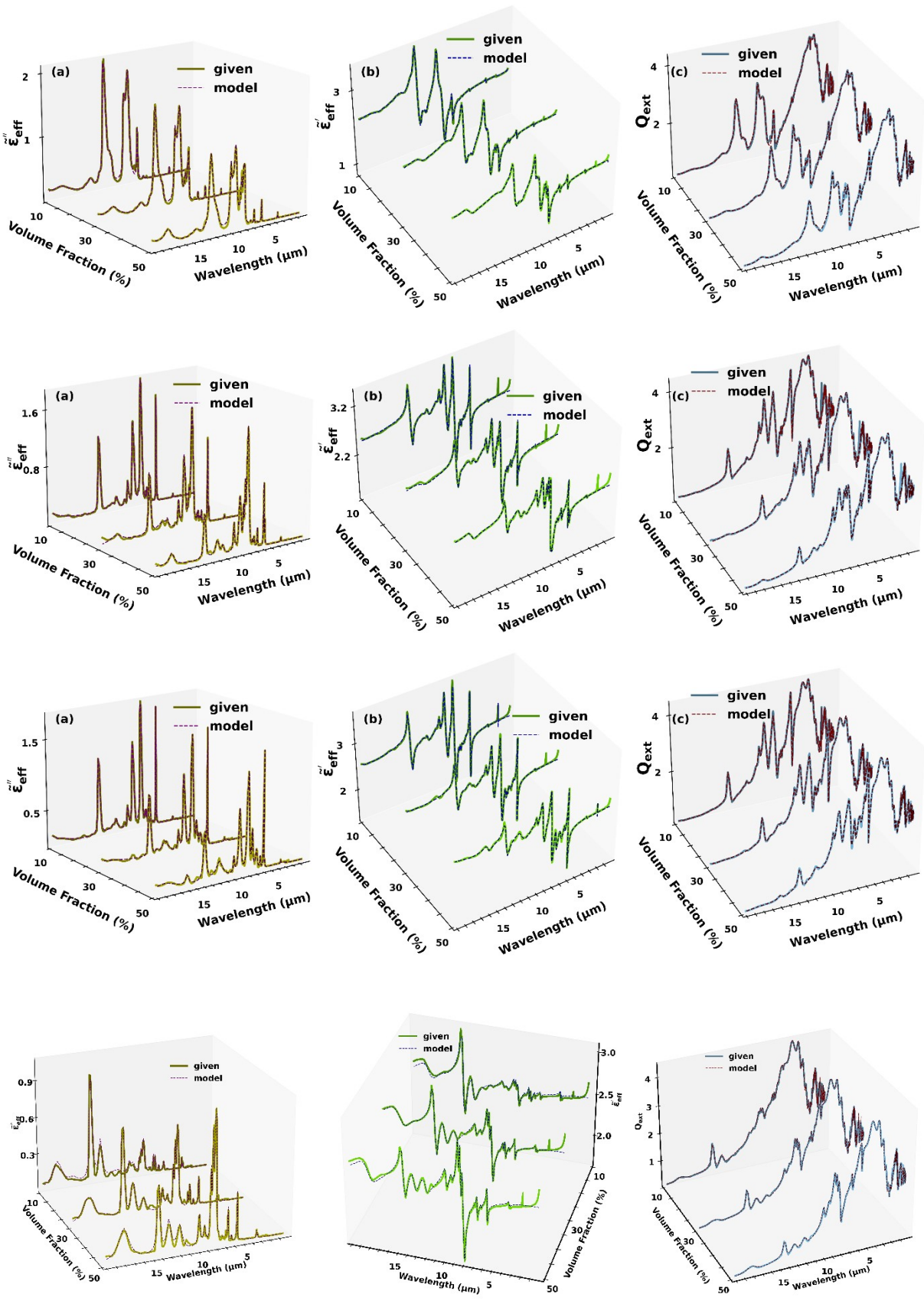
(a)
(b)
(c)
given
model
Volume Fraction (%)
Wavelength (μm)
$\tilde{\varepsilon}''_{eff}$
$\tilde{\varepsilon}'_{eff}$
Q_{ext}

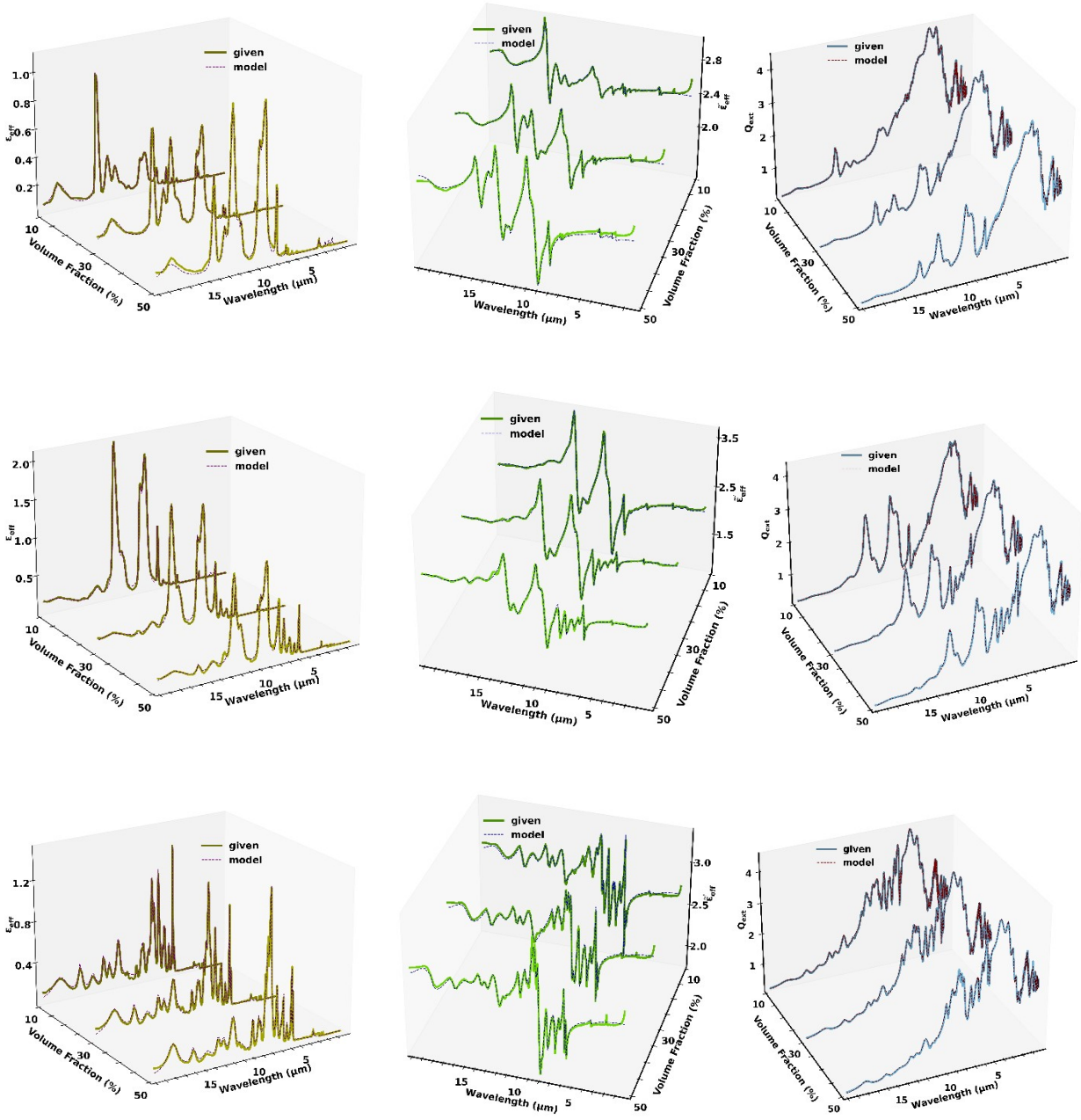
given
model
Volume Fraction (%)
Wavelength (μm)
Qext

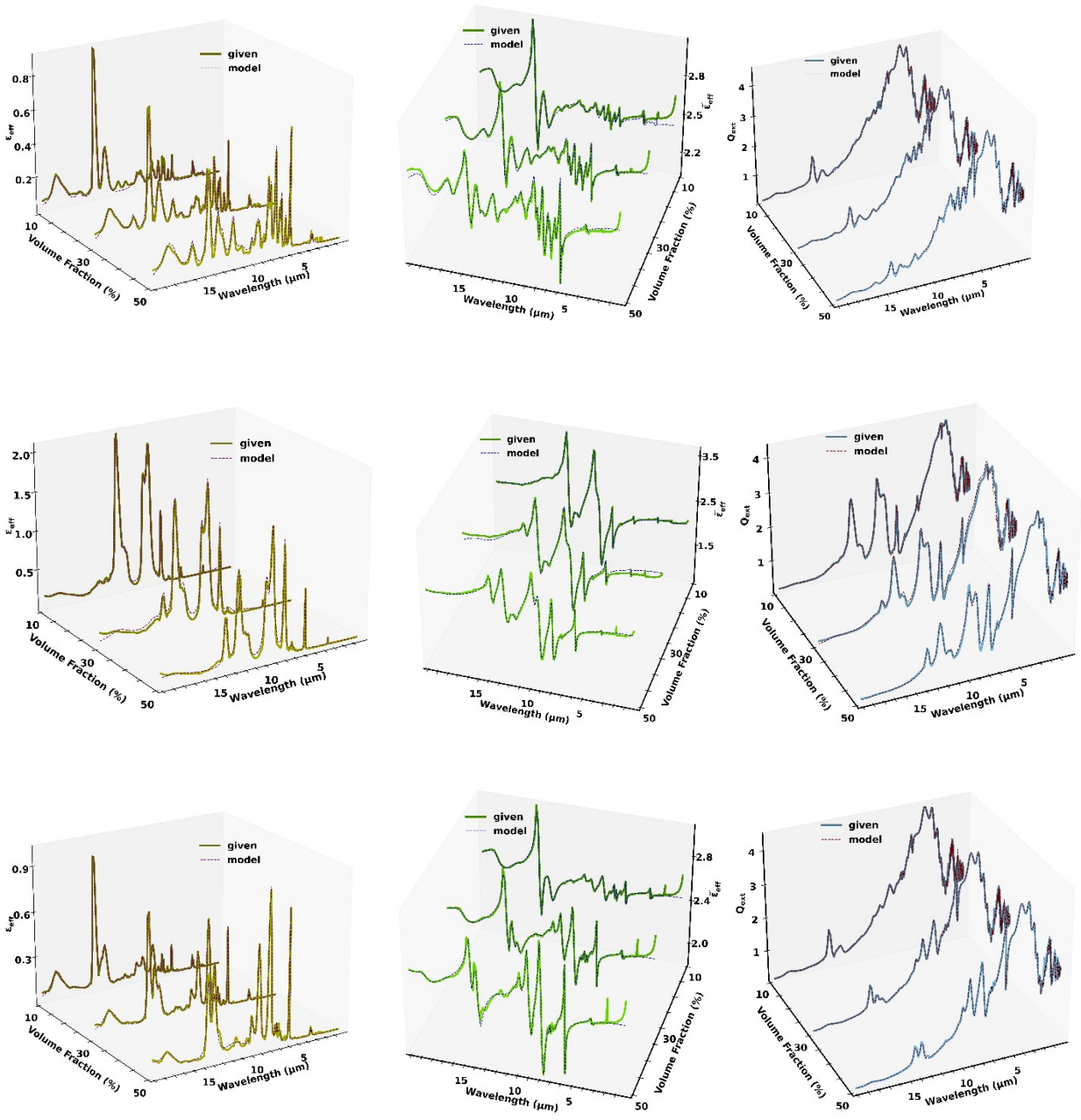
given
model
Volume Fraction (%)
Wavelength (μm)
ε_{eff}
$\tilde{\varepsilon}_{eff}$
Q_{ext}

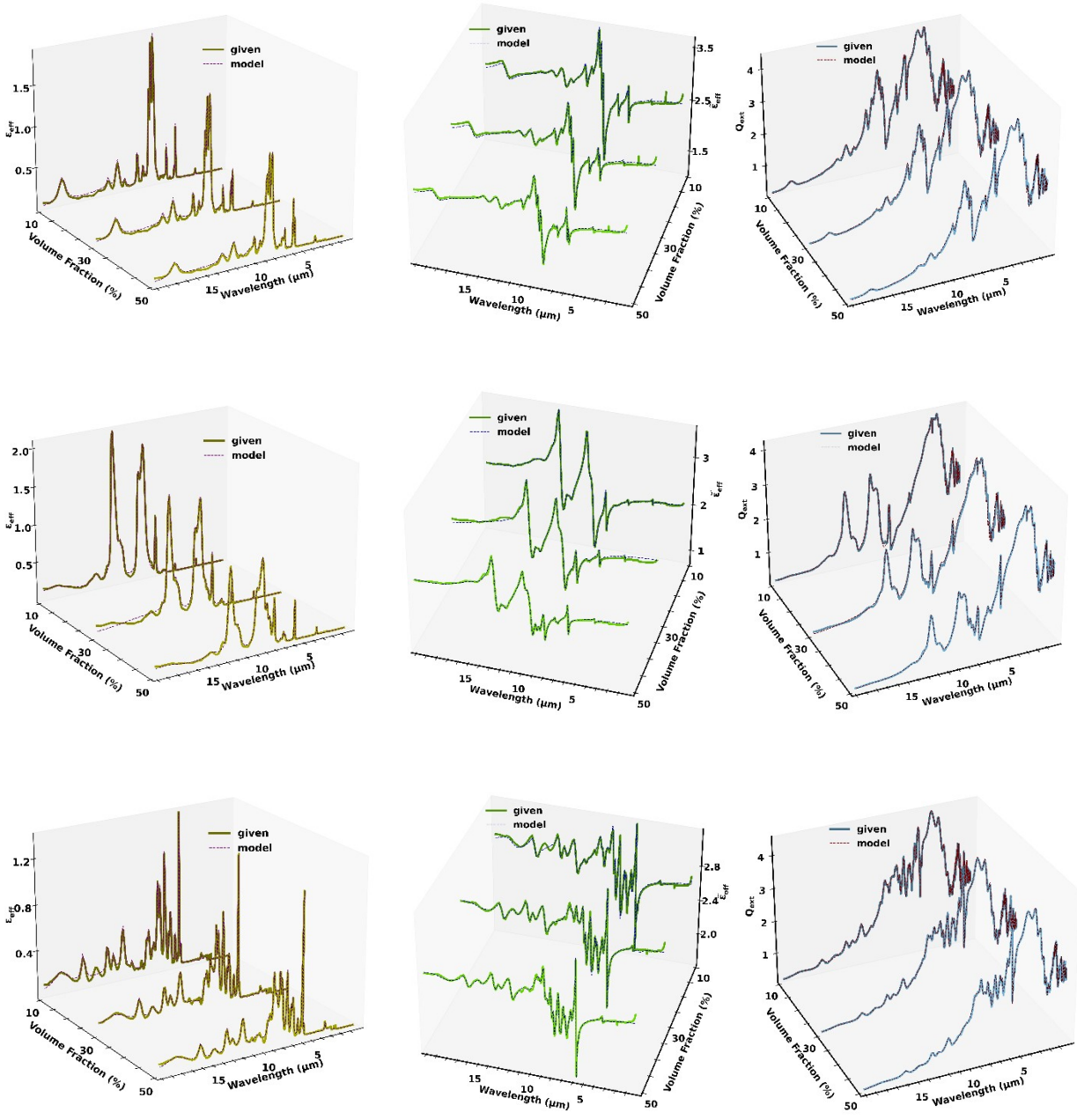
given
model
Volume Fraction (%)
Wavelength (μm)
ε_{eff}
Q_{ext}

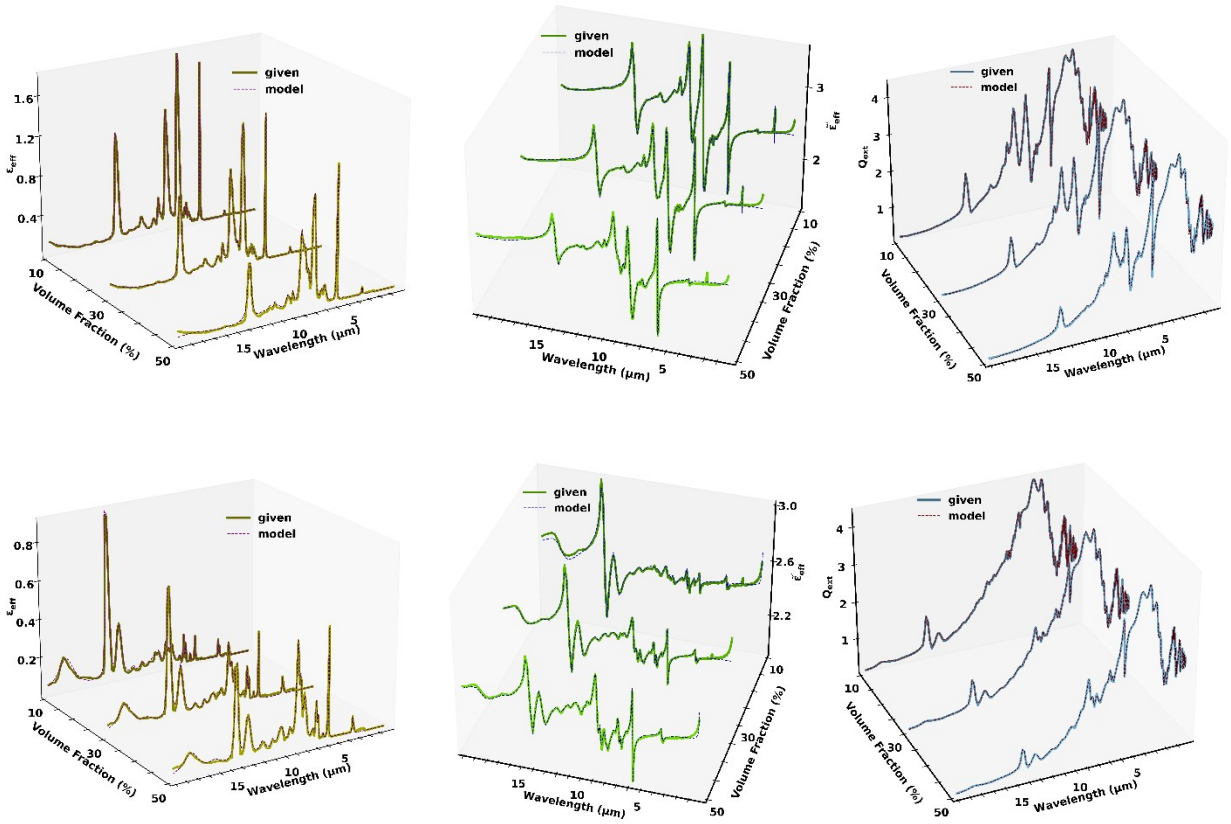

Figure S3 Compares the **(a)** imaginary (solid pale yellow) part of the experimental complex effective permittivity, $\tilde{\epsilon}_{eff}^{''}$, to the imaginary (dashed yellow) part of the fit of the complex effective permittivity, $\tilde{\epsilon}_{eff}^{''(model)}$, **(b)** real (solid pale green) part of the experimental complex effective permittivity, $\tilde{\epsilon}_{eff}^{'}$, to the real (dashed dark blue) part of the fit of the complex effective permittivity, $\tilde{\epsilon}_{eff}^{'(model)}$, and **(c)** experimental effective extinction efficiency (solid light blue), $Q_{ext}^{(given)}$, to the numerical fit of the effective extinction efficiency (dashed dark red), $Q_{ext}^{(model)}$, respectively, for three two-component cubic mixtures, each composed of $10\% - 90\%$, $30\% - 70\%$, and $50\% - 50\%$ of **A)** PC-PDMS, **B)** PC-PET, **C)** PEI-PET, **D)** PC-PS, **E)** PDMS-PS, **F)** PEI-PDMS, **G)** PC-PEI, **H)** PEI-PS, **I)** PET-PDMS, **J)** PET-PS, **K)** PMMA-PC, **L)** PMMA-PDMS, **M)** PMMA-PEI, **N)** PMMA-PET, and **O)** PMMA-PS, respectively.

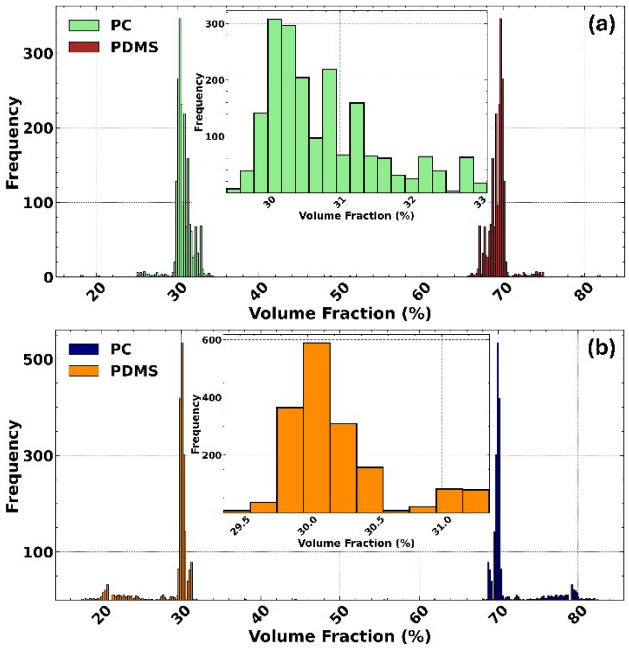

Figure S4 *Inverted mixing rule reconstructions of the volume fractions of a* 30%:70% *PC–PDMS two-component mixture were performed using* 2000 *randomly chosen initial conditions. The search algorithms employed were:* ***(a)*** *grid search and* ***(b)*** *gradient descent, respectively.*

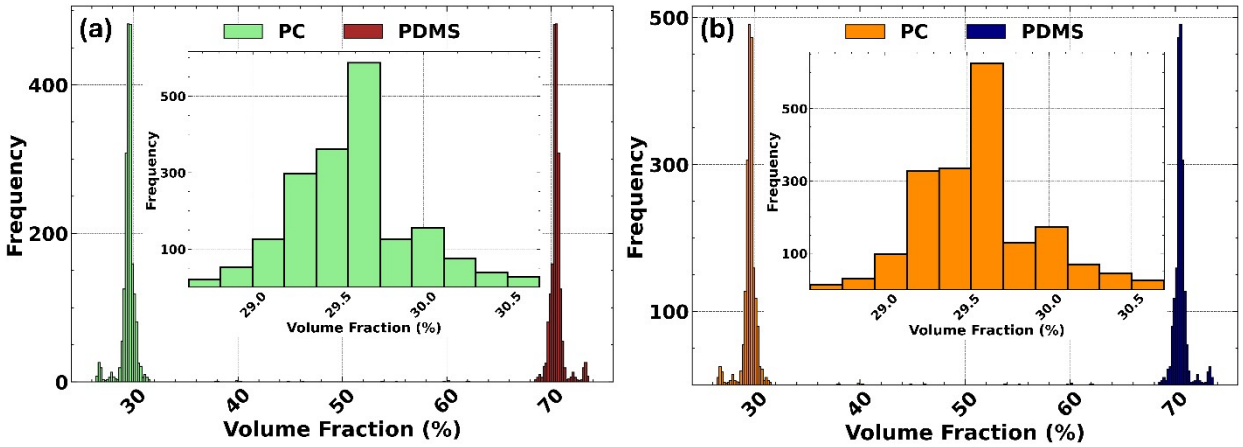

Figure S5 *Logarithmic mixing rule reconstructions of the volume fractions of a* 30%:70% *PC–PDMS two-component mixture were performed using* 2000 *randomly chosen initial conditions. The search algorithms employed were:* ***(a)*** *grid search and* ***(b)*** *gradient descent, respectively.*

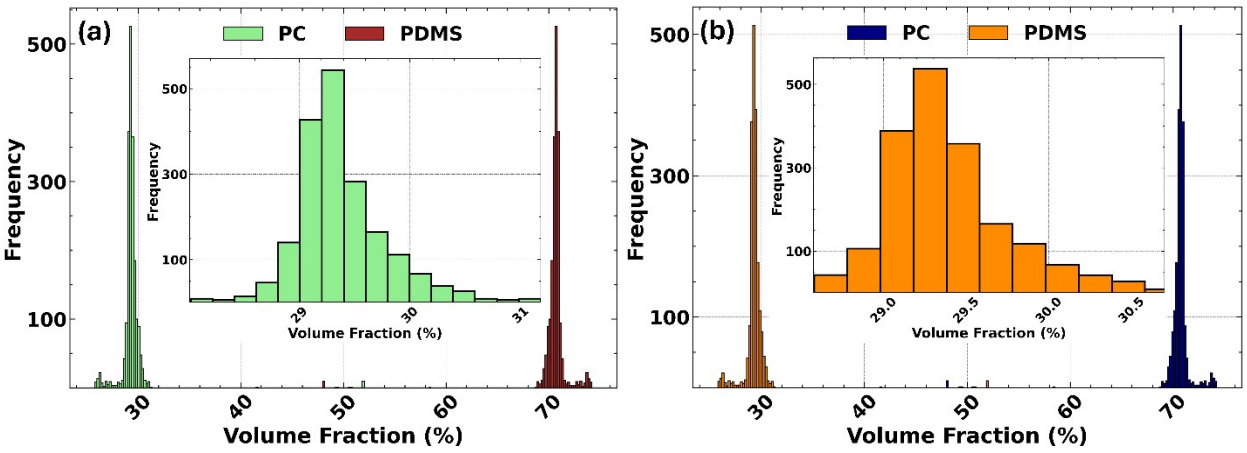

Figure S6 *Cubic mixing rule reconstructions of the volume fractions of a* 30%:70% *PC–PDMS two-component mixture were performed using* 2000 *randomly chosen initial conditions. The search algorithms employed were:* ***(a)*** *grid search and* ***(b)*** *gradient descent, respectively.*

Table S1: Validation of Microstructure Diagnosis (Two-Component Mixtures). *Matrix showing the residual sum of squares (RSS) when the complex effective permittivity of two-component blends (PC-PDMS at* 10%:90%, 30%:70%, *and* 50%:50% *volume fraction) is deconvolved by competing inverse topological models. For a successful diagnosis, the inverse model with the lowest RSS must match the input topology used to generate the forward spectrum. The consistent minimization of the RSS confirms the diagnostic fidelity of the framework for both the grid search (GS) and gradient descent (GD) algorithms.*

Polymer Blend	Volume Fraction (%)	Input Topology (Forward Model)	Inverse Topology (Reconstructed)	RSS	
				Grid Search	Gradient Descent
PC-PDMS	10%:90%	Inverted	Inverted	0.32 **(Lowest)**	0.32 **(Lowest)**
			Logarithmic	0.44	0.44
			Cubic	0.52	0.53
			Linear	0.77	0.82
		Logarithmic	Inverted	0.46	0.47
			Logarithmic	0.33 **(Lowest)**	0.34 **(Lowest)**
			Cubic	0.36	0.36
			Linear	0.53	0.56
		Cubic	Inverted	0.55	0.56
			Logarithmic	0.48	0.49
			Cubic	0.45 **(Lowest)**	0.45 **(Lowest)**
			Linear	0.64	0.66
	30%:70%	Inverted	Inverted	0.32 **(Lowest)**	0.32 **(Lowest)**
			Logarithmic	1.18	1.21
			Cubic	1.82	1.91
			Linear	3.68	4.07
		Logarithmic	Inverted	1.51	1.65
			Logarithmic	0.77 **(Lowest)**	0.95 **(Lowest)**
			Cubic	0.99	1.25
			Linear	2.19	2.77
		Cubic	Inverted	2.12	2.18
			Logarithmic	0.52	0.57
			Cubic	0.41 **(Lowest)**	0.43 **(Lowest)**
			Linear	0.92	0.93
	50%:50%	Inverted	Inverted	0.35 **(Lowest)**	0.33 **(Lowest)**

			Logarithmic	2.07	2.18
			Cubic	3.35	3.57
			Linear	6.97	7.62
		Logarithmic	Inverted	2.17	2.30
			Logarithmic	0.54 **(Lowest)**	0.54 **(Lowest)**
			Cubic	0.79	0.80
			Linear	2.39	2.55
		Cubic	Inverted	3.73	4.05
			Logarithmic	0.83	0.87
			Cubic	0.68 **(Lowest)**	0.68 **(Lowest)**
			Linear	1.51	1.56

Table S2: Validation of Microstructure Diagnosis (Multi-Component Mixtures). *Matrix showing the residual sum of squares (RSS) when the complex effective permittivity of multi-component blends (PMMA-PC-PDMS-PET-PEI-PS at* 40%:10%:5%:15%:20%:10%, 30%:20%:10%:5%:15%:20%, 5%:5%:65%:5%:5%:15%, 0%:0%:78%:3%:7%:12%, 19%:13%:41%:8%:18%:1%, *and* 16.5%:16.5%:16.5%:16.5%:16.5%:17.5% *volume fraction) is deconvolved by competing inverse topological models. For a successful diagnosis, the inverse model with the lowest RSS must match the input topology used to generate the forward spectrum. The consistent minimization of the RSS confirms the diagnostic fidelity of the framework for the gradient descent (GD) algorithm.*

Polymer Blend	Volume Fraction (%)	Input Topology (Forward Model)	Inverse Topology (Reconstructed)	RSS
				Gradient Descent
PMMA-PC-PDMS-PET-PEI-PS	40%:10%:5%:15%:20%:10%	Inverted	Inverted	0.23 **(Lowest)**
			Logarithmic	0.48
			Cubic	0.58
			Linear	0.78
		Logarithmic	Inverted	2.15
			Logarithmic	1.24 **(Lowest)**
			Cubic	1.34
			Linear	1.30
		Cubic	Inverted	1.46
			Logarithmic	0.80
			Cubic	0.71 **(Lowest)**
			Linear	0.86
	30%:20%:10%:5%:15%:20%	Inverted	Inverted	0.26 **(Lowest)**
			Logarithmic	0.74
			Cubic	0.95
			Linear	1.29
		Logarithmic	Inverted	0.51
			Logarithmic	0.10 **(Lowest)**
			Cubic	1.37
			Linear	0.30
		Cubic	Inverted	0.73
			Logarithmic	0.12
			Cubic	0.10 **(Lowest)**
			Linear	0.19
	5%:5%:65%:5%:5%:15%	Inverted	Inverted	0.27 **(Lowest)**
			Logarithmic	1.00
			Cubic	1.54
			Linear	2.93
		Logarithmic	Inverted	1.11
			Logarithmic	0.28 **(Lowest)**
			Cubic	0.36
			Linear	0.95

		Cubic	Inverted	2.80
			Logarithmic	1.91
			Cubic	1.28 **(Lowest)**
			Linear	2.06
	0%:0%:78%:3%:7%:12%	Inverted	Inverted	0.28 **(Lowest)**
			Logarithmic	0.61
			Cubic	0.89
			Linear	1.71
		Logarithmic	Inverted	1.71
			Logarithmic	0.86 **(Lowest)**
			Cubic	2.36
			Linear	3.06
		Cubic	Inverted	2.45
			Logarithmic	0.88
			Cubic	0.84 **(Lowest)**
			Linear	1.35
	19%:13%:41%:8%:18%:1%	Inverted	Inverted	0.17 **(Lowest)**
			Logarithmic	1.69
			Cubic	2.61
			Linear	4.74
		Logarithmic	Inverted	2.27
			Logarithmic	0.26 **(Lowest)**
			Cubic	0.33
			Linear	1.14
		Cubic	Inverted	4.10
			Logarithmic	0.63
			Cubic	0.35 **(Lowest)**
			Linear	0.64
	16.5%:16.5%:16.5%:16.5%:16.5%:17.5%	Inverted	Inverted	0.42 **(Lowest)**
			Logarithmic	1.48
			Cubic	1.89
			Linear	2.59
		Logarithmic	Inverted	0.94
			Logarithmic	0.17 **(Lowest)**
			Cubic	0.24
			Linear	0.57
		Cubic	Inverted	1.50
			Logarithmic	0.20
			Cubic	0.15 **(Lowest)**
			Linear	0.32

Table S3: *Mixture deconvolution using grid search and gradient descent to identify individual components and volume fractions in two-component mixtures governed by inverted, logarithmic, and cubic mixing rules.*

Material	**Volume Fraction (%)**	**Reconstructed Mixture (Grid Search) (%)**			**Reconstructed Mixture (Gradient Descent) (%)**		
		Inverted	**Logarithmic**	**Cubic**	**Inverted**	**Logarithmic**	**Cubic**
PC-PDMS	10:90	10.3:89.7	10.2:89.8	9.2:90.8	10.3:89.7	10.2:89.8	9.2:90.8
	30:70	30.2:69.8	29.4:70.6	30.1:69.9	30.2:69.8	29.4:70.6	30.1:69.9
	50:50	50.0:50.0	49.8:50.2	49.8:50.2	50.0:50.0	49.8:50.2	49.8:50.2
PC-PEI	10:90	10.3:89.7	10.5:89.5	10.4:89.6	10.3:89.7	10.5:89.5	10.4:89.6
	30:70	30.6:69.4	30.6:69.4	30.7:69.3	30.6:69.4	29.6:70.4	30.7:69.3
	50:50	49.3:50.7	50.8:49.2	48.9:51.1	49.3:50.7	49.0:51.0	48.9:51.1
PC-PET	10:90	10.4:89.6	10.6:89.4	10.3:89.7	10.4:89.6	10.6:89.4	10.3:89.7
	30:70	30.9:69.1	30.2:69.8	29.9:70.1	30.9:69.1	30.2:69.8	29.9:70.1
	50:50	50.1:49.9	49.9:50.1	50.5:49.5	50.1:49.9	49.9:50.1	50.5:49.5
PEI-PDMS	10:90	10.5:89.5	10.6:89.4	11.0:89.0	10.5:89.5	10.6:89.4	11.0:89.0
	30:70	30.1:69.9	30.4:69.6	30.0:70.0	30.1:69.9	30.4:69.6	30.0:70.0

	50:50	49.9:50.1	49.9:50.1	49.7:50.3	49.9:50.1	49.9:50.1	49.7:50.3
PEI-PET	10:90	10.1:89.9	10.5:89.5	11.6:88.4	10.1:89.9	10.5:89.5	11.6:88.4
	30:70	29.7:70.3	29.5:70.5	30.2:69.8	29.7:70.3	29.5:70.5	30.2:69.8
	50:50	50.0:50.0	49.9:50.1	50.0:50.0	50.0:50.0	49.9:50.1	50.0:50.0
PET-PDMS	10:90	10.2:89.8	10.7:89.3	10.1:89.9	10.2:89.8	10.7:89.3	10.1:89.9
	30:70	29.9:70.1	29.8:70.2	28.4:71.6	29.9:70.1	29.8:70.2	28.4:71.6
	50:50	49.6:50.4	50.0:50.0	49.4:50.6	49.6:50.4	50.0:50.0	49.4:50.6
PMMA-PC	10:90	9.7:90.3	10.5:89.5	9.0:91.0	9.7:90.3	10.5:89.5	9.0:91.0
	30:70	29.5:70.5	29.6:70.4	28.6:71.4	29.5:70.5	29.6:70.4	28.6:71.4
	50:50	49.6:50.4	49.5:50.5	48.8:51.2	49.6:50.4	49.5:50.5	48.8:51.2
PMMA-PDMS	10:90	10.5:89.5	10.5:89.5	10.1:89.9	10.5:89.5	10.5:89.5	10.1:89.9
	30:70	30.2:69.8	30.6:69.4	28.7:71.3	30.2:69.8	30.6:69.4	28.7:71.3
	50:50	50.0:50.0	50.0:50.0	49.6:50.4	50.0:50.0	50.0:50.0	49.6:50.4
PMMA-PEI	10:90	10.8:89.2	11.7:88.3	10.6:89.4	10.8:89.2	11.7:88.3	10.6:89.4
	30:70	31.3:68.7	32.6:67.4	31.2:68.8	31.3:68.7	32.6:67.4	31.2:68.8
	50:50	50.1:49.9	51.8:48.2	50.3:49.7	50.1:49.9	51.8:48.2	50.3:49.7
PMMA-PET	10:90	10.2:89.8	10.1:89.9	10.4:89.6	10.2:89.8	10.1:89.9	10.4:89.6
	30:70	30.4:69.6	30.6:69.4	30.4:69.6	30.4:69.6	30.6:69.4	30.4:69.6
	50:50	50.1:49.9	50.0:50.0	49.6:50.4	50.1:49.9	50.0:50.0	49.6:50.4
PMMA-PS	10:90	11.4:88.6	8.9:91.1	10.2:89.8	11.3:88.7	8.9:91.1	10.2:89.8
	30:70	31.1:68.9	30.3:69.7	29.4:70.6	31.1:68.9	30.3:69.7	29.4:70.6
	50:50	50.3:49.7	50.5:49.5	50.1:49.9	50.3:49.7	50.5:49.5	50.1:49.9
PC-PS	10:90	10.2:89.8	9.5:90.5	11.2:88.8	10.2:89.8	9.5:90.5	11.2:88.8
	30:70	29.8:70.2	29.6:70.4	29.7:70.3	29.8:70.2	29.6:70.4	29.7:70.3
	50:50	50.5:49.5	49.0:51.0	50.6:49.4	50.5:49.5	49.0:51.0	50.6:49.4
PDMS-PS	10:90	10.3:89.7	10.2:89.8	10.0:90.0	10.3:89.7	10.2:89.8	10.0:90.0
	30:70	30.4:69.6	30.0:70.0	29.7:70.3	30.4:69.6	30.0:70.0	29.7:70.3
	50:50	50.2:49.8	50.2:49.8	48.5:51.5	50.2:49.8	50.2:49.8	48.5:51.5
PEI-PS	10:90	11.5:88.5	10.9:89.1	7.5:92.5	11.5:88.5	10.9:89.1	7.5:92.5
	30:70	30.3:69.7	30.6:69.4	30.5:69.5	30.3:69.7	30.6:69.4	30.5:69.5
	50:50	50.1:49.9	50.2:49.8	50.9:49.1	50.1:49.9	50.2:49.8	50.9:49.1
PET-PS	10:90	10.7:89.3	9.2:90.8	9.9:90.1	10.7:89.3	9.2:90.8	9.9:90.1
	30:70	29.9:70.1	30.4:69.6	29.8:70.2	29.9:70.1	30.4:69.6	29.8:70.2
	50:50	50.3:49.7	49.5:50.5	50.0:50.0	50.3:49.7	49.5:50.5	50.0:50.0

Table S4: *Mixture deconvolution using gradient descent to identify individual components and volume fractions in six multi-component mixtures governed by inverted, logarithmic, and cubic mixing rules.*

Material	**Volume Fraction (%)**	**Reconstructed Mixture (%)**		
		Inverted	**Logarithmic**	**Cubic**
PMMA-PC-PDMS-PET-PEI-PS	40:10:5:15:20:10	39.9:10.3:5.3:14.6:20.1:9.8	41.2:9.4:4.4:15.1:18.1:11.7	41.3:9.3:4.4:14.9:18.7:11.4
	30:20:10:5:15:20	30.0:20.3:10.3:4.9:14.4:20.2	29.8:20.3:10.3:4.8:14.4:20.4	29.7:20.4:10.4:4.8:14.8:19.9
	5:5:65:5:5:15	7.9:5.2:65.4:4.1:3.6:13.8	7.7:4.5:64.8:4.6:1.9:16.5	5.0:6.0:66.0:4.2:9.1:9.7
	0:0:78:3:7:12	1.5:0.0:78.1:3.5:5.4:11.5	0.0:0.0:76.7:3.1:7.6:12.7	1.3:0.6:78.7:2.2:9.4:7.8
	19:13:41:8:18:1	20.0:13.5:41.3:7.1:17.3:0.8	20.2:13.1:40.8:7.5:15.9:2.5	20.1:12.9:40.5:7.7:16.1:2.7

	16.5:16.5:16.5:16.5:16.5:17.5	19.0:16.6:16.8:16.3:14.8:16.6	17.0:16.5:16.8:16.0:15.8:18.1	16.3:16.3:16.8:16.0:16.7:17.8